JOURNAL OF MATERIALS SCIENCE **34** (1999) 2475–2481

Chronological evaluation of interfacial damage in TBC due to thermal cycling

Z. A. CHAUDHURY*, G. M. NEWAZ*, S. Q. NUSIER*, T. AHMED‡, R. L. THOMAS‡
Mechanical Engineering Department, ‡Institute for Manufacturing Research, Wayne State University, Detroit, MI 48202, USA

A two layer electron beam-physical vapor deposited (EV-PVD) thermal barrier coating (TBC) on a single crystal superalloy (René N5) substrate was characterized prior to and after thermal cycling at 2, 18, 25, 44, 50, 75, 100, 110, 150, and 175 cycles in between 200 C-1177 C. Optical microscopy, scanning electron microscopy, and thermal wave imaging techniques were used to characterize the interfacial damage. Pt-Al was used as bond coat and 8 wt % YSZ was used as outer top layer. Interfacial cracking was observed even at two thermal cycles. Thermally grown oxide (TGO) layer increased with the number of thermal cycles. After numerous cycles over 100, interfacial separation was observed to be higher at the middle than at the edges of the sample. This observation is consistent with buckling induced delamination—a possible mechanism for spallation.

1. Introduction

Different turbine engine components use thermal barrier coatings (TBCs) to increase the life of the metal parts and to improve the operating temperature. TBCs offer a number of benefits including up to 145 °C metal temperature reduction, significant fuel savings and improved durability [1, 2]. Other advantages and improvements of TBCs on the turbine blades are the increase in the turbine thermal efficiency due to a higher stator outlet temperature, the increase in the compressor efficiency due to a reduced air flow for the turbine cooling, and a longer service life for the metallic substrate due to a decreased thermal fatigue load. TBCs consist of a thermally insulating zirconia ceramic overlayer applied over a metallic bond coat, which protects the substrate from oxidation and hot corrosion during high temperature operations.

Several coating methods are available. Of them plasma spray and electron-beam physical vapor deposition (EB-PVD) processes are very popular for their various advantages. EB-PVD has been successfully used to coat turbine airfoils [3]. EB-PVD ceramic structure is highly columnar, the columns are aligned perpendicular to the metal-ceramic interface. Due to columnar microstructure in EB-PVD system, the coatings become strain tolerant. The reason for this is that the coatings can accommodate the applied thermal strain by movement between the columnar growth structures [2]. In the EB-PVD technique, a small piece of ceramic material such as 8 wt % YSZ is evaporated by an electron beam in a vacuum chamber. The ceramic vapor cloud condenses on the surfaces of the component, which is rotated and controlled in the vapor cloud to form the coating. Power to evaporate the ceramic coating material is provided by a high-energy electron beam gun. Feeders, electron beam gun, temperature, and gas should be controlled very carefully.

Calculations indicate that a 0.25 mm thick layer of zirconia can reduce metal temperature by as much as 170 °C depending on local heat flux [1, 4]. This relative temperature reduction can provide significant benefits [1, 2] in the form of either component durability extension or system performance improvement. The most widely used TBCs are based on zirconia (zirconium dioxide), which shows thermal expansion characteristic similar to superalloys. Zirconia offers a good compromise with a low thermal conductivity of about 2 W/mK and a high thermal expansion coefficient ($\sim 10 \times 10^{-6}\,K^{-1}$) [5]. Yttria stabilized zirconia (YSZ) coatings represent the current state of the art of TBCs [6].

Bond coat compositions started from early Ni—Cr and Ni—Al compositions to the presently used MCrAlX (M=Ni or Cr or both, X=Hf, Zr or Al) and Pt—Al compositions. Pt—Al diffusion coating has been developed due to demands on coatings for gas turbine engines, which must operate at significantly higher temperatures than required previously. Oxidation behavior of platinum-modified aluminide coating and platinum–aluminum alloys has been reported by other investigators [7, 8].

The function of the bond coat in a TBC system is to provide good adhesion between the metal substrate and the ceramic top coat while providing good oxidation protection to the underlying substrate alloy. During thermal exposure, this bond coat oxidizes and forms an aluminum oxide layer between the ceramic and the bond coat. Oxidation plays a dominant role in the failure of graded thermal barrier coatings as confirmed by many researchers [9–12]. Oxidation of the bond coat

has been proposed [13] as a life limiting factor of TBCs. Numerous studies have shown that oxidation of bond coat can significantly affect spalling [14–17].

Depending on the temperature range to which thermal barrier coatings are exposed, different types of failure modes have been observed. Bond coat oxidation and damage initiation is common for high temperature applications [18–20]. On the other hand, for low temperature applications, thermal cyclic stresses that occur during engine operation is believed to be responsible for coating delamination and spallation [21]. For long-term successful use of the turbine components, the durability of the TBC must be maintained. Due to improvements in processing condition and coating materials, significant advances in coating durability have been realized [22–28]. Stress calculations have indicated that high rates of heating and cooling have a more destructive influence on ceramic coating life than isothermal exposure at temperature [29]. Substrate temperature is important in TBC behavior. Thermal cycle life of TBC decreases dramatically due to higher substrate temperature [30–31]. Compressive stresses are also believed to be responsible for TBC failure, which occur in the ceramic layer during cooling [14, 29]. The mechanism involves buckling of TBC due to compressive residual stress, which results in spallation. These stresses can be attributed to the thermal expansion mismatch between the ceramic top coat and the metal bond coat [32–35]. Extensive research work on TBCs have been reported in the literature [36–46]. The basic causes of TBC failure and the effect of TGO on delamination is still not clear. As a part of our continued research program on an investigation with focus on damage accumulation mechanisms in thermal barrier coated single crystal substrate [47–49], a number of thermal cycling tests have been carried out, evaluated, and analyzed to determine the causes of coating failure and delamination. In this article, we present a chronological sequence of damage and oxidation evolution at the bond coat and TBC interface.

2. Experimental procedure

The TBC specimens were 25.4 mm in diameter by 3.17 mm thick button samples of nickel base superalloy Rene' N5. There are two coats: one is the top coat, which is the EB-PVD thermally insulting outer ceramic layer, and the other is the bond coat, which is a diffusion aluminide Pt-Al alloy. The outer layer TBC was the 8 % wt YSZ. The thickness of the outer top coat is 0.127 mm, and that of bond coat is 0.0482 mm. Several researchers have worked on this material system between 150 C-1200 C. A number of coated specimens were placed in a muffle-type rapid heating/cooling furnace and thermally cycled to 2, 18, 25, 42, 50, 75, 100, 110, 150, and 175 cycles in the range of (200 °C–1177 °C). The holding time was 45 minutes at the peak temperature in each cycle. The rate of heating was nine minutes to reach to the peak temperature and the rate of cooling was 10 minutes to reach to the lower temperature of the cycles. Fig. 1 shows the temperature profile of the thermal cycle tests.

A number of samples were taken out after a certain number of thermal cycles. These samples did not fail.

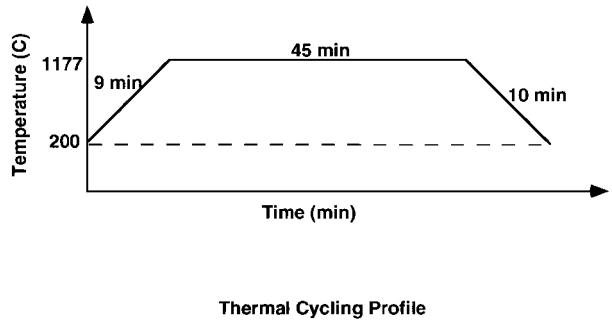

Figure 1 The temperature profile of the thermal cycle tests conducted in the present investigation.

The thermally cycled samples were cold mounted using epoxide resin. The samples were sectioned, ground, and polished using normal metallurgical procedures. The polished samples were observed under Olympus BX 60 optical microscope. Scanning electron microscopy was carried by using a Hitachi 2000 SEM on the polished samples to observe interfacial damage/crack propagation at the ceramic top coat and bond coat interface and morphology of the thermally grown oxide (TGO) layer at higher magnification.

Thermal wave images were taken on the surface of the thermally cycled and untested samples in order to identify any damage at the ceramic top coat and bond coat interface. The thermal wave imaging method is based on the idea that a time-dependent heat source at the surface of an object launches waves of heat into the object in the form of heat diffusion, called thermal waves. The thermal waves are scattered from subsurface defects or anomalies in much the same way that sound waves reflect from such defects and, upon returning to the surface of the object, modify the temperature of the surface map. In the usual configuration, high-power flash lamps are used to pulse-heat the surface of the object under inspection. This causes a plane thermal wave pulse to propagate into the material from the heated surface. As this pulse encounters subsurface material defects, each defect scatters a fraction of the pulse back towards the surface. When these scattered pulses or thermal waves arrive back at the surface, they modify the time-dependent temperature distribution on the surface, with signal from defects at different depths affecting the surface temperature at different times. During the process, the evolving surface temperature distribution is imaged by an infrared video camera as a function of time. Through the use of fast image processing hardware and software, the system's computer memory stores a sequence of gated images corresponding to the various times after the flash heating. The result is a series of thermal wave images corresponding to various depths beneath the surface. The time after the onset of the flash heating at which defects from various depths beneath the surface can be observed depends on the depth and the thermal diffusivity of the specimen under inspection.

3. Results and discussions

3.1. Thermal cycling of TBC samples

Fig. 2 shows the photomicrograph of a thermal barrier coated sample without any thermal cycling. No

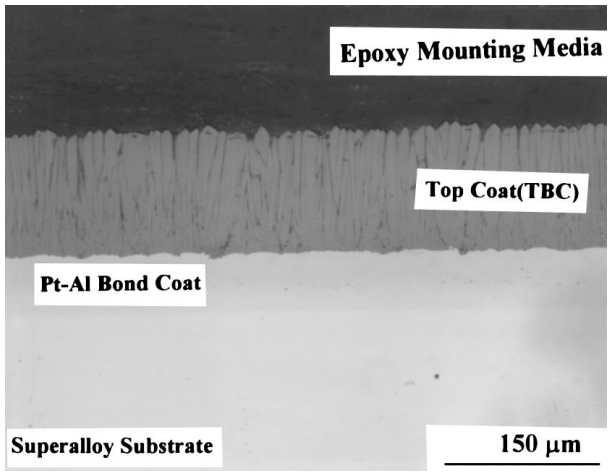

Figure 2 An optical micrograph of an untested thermal barrier coated sample. Thermally Grown Oxide (TGO) layer and/or interfacial separation were absent at the bond coat/top coat (TBC) interface.

interfacial cracking and oxidation product (TGO) was observed at the bond coat/top coat (TBC) interface. Thermally cycled TBC samples in air leads to the formation of a reaction product layer and interfacial cracking/damage at the bond coat/top coat interface. This oxidation product (TGO) is Al_2O_3 and has been confirmed by many researchers [47, 48, 51, 52]. Interdiffusion of bond coat and substrate elements at elevated temperature does occur [53], and their effect on TBC failure is still not clear. Migration of aluminum from bond coat into the substrate can change the oxidation behavior of the bond coat and sometimes may be responsible for the formation of less adherent oxide species. A few thermal cycles lead to the formation of interfacial cracking at the bond coat/top coat interface, and increasing the number of cycles leads to the formation of both interfacial cracking and TGO layer. Fig. 3a and b shows the photomicrographs of the interfacial cracking at the bond coat/top coat interface taken after 2 and 18 thermal cycles. TGO layer just started growing at 18 thermal cycles. The length of the interfacial crack was typically 600 μm and the thickness of the crack was 3 μm. The TGO layer starts growing with increasing the number of thermal cycles. Fig. 3c and d, Fig. 4a–c, Fig. 5, and Fig. 6a and b show the chronological evaluation of interfacial damage in TBC due to thermal cycling at 25, 42, 50, 75, 100, 110, and 175 cycles. The thickness of the TGO layer grows as the number of cycles increases. Fig. 4c shows separation through the TGO layer. In Fig. 5, interfacial cracking at the bond coat/top coat interface are increased and TGO layer is quite visible through the interfacial cracking. Interfacial cracking is showing a sinusoidal nature. In Fig. 6a and b, complete separation through the TGO layer is observed. This TGO layer/separation is very high at the center

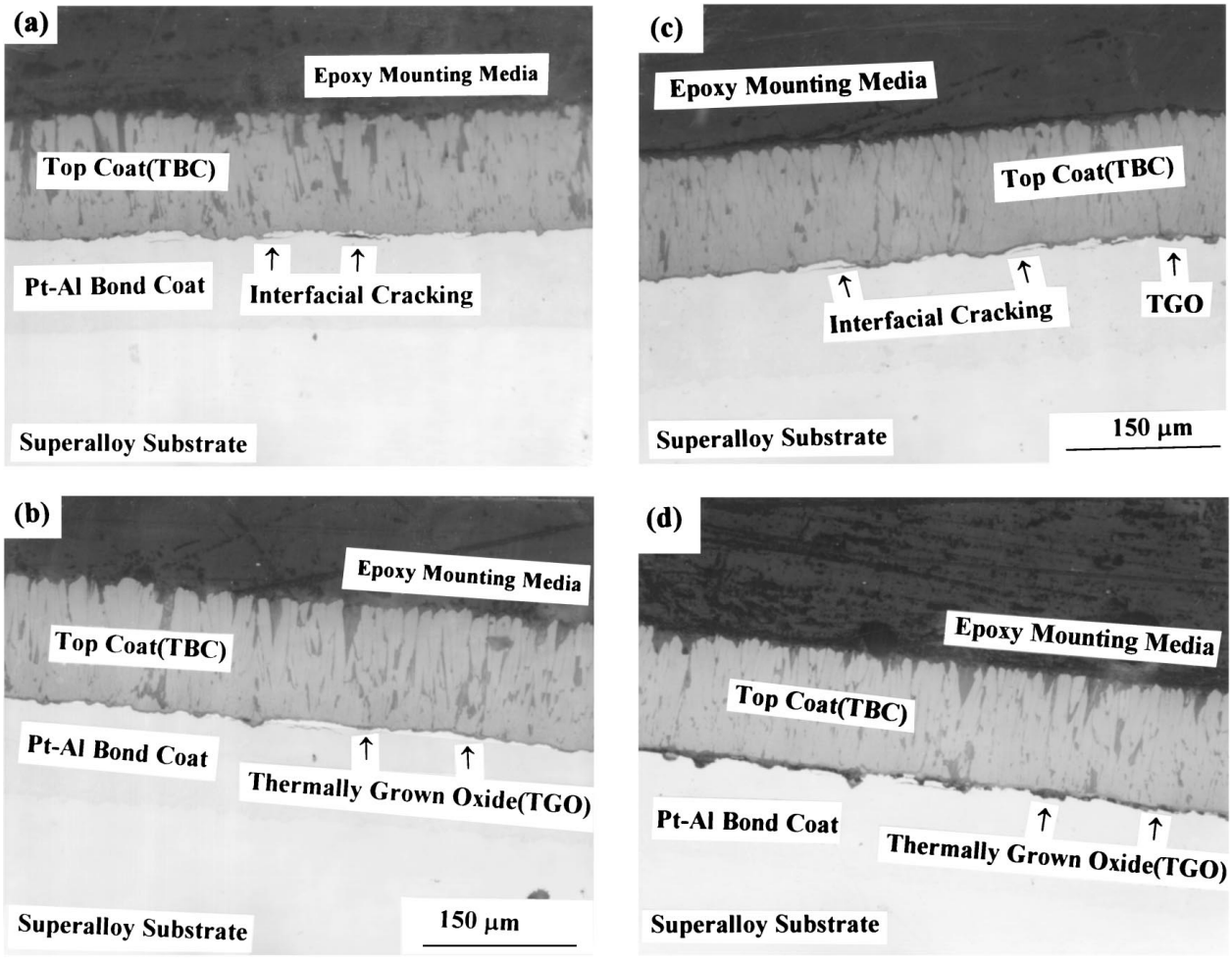

Figure 3 (a) and (b) Photomicrographs of interfacial cracking at the bond coat/top coat interface taken after 2 and 18 thermal cycles. TGO layer started growing at 18 cycles, (c) and (d) chronological evaluation of interfacial damage in TBC due to thermal cycling at 25 and 42 cycles.

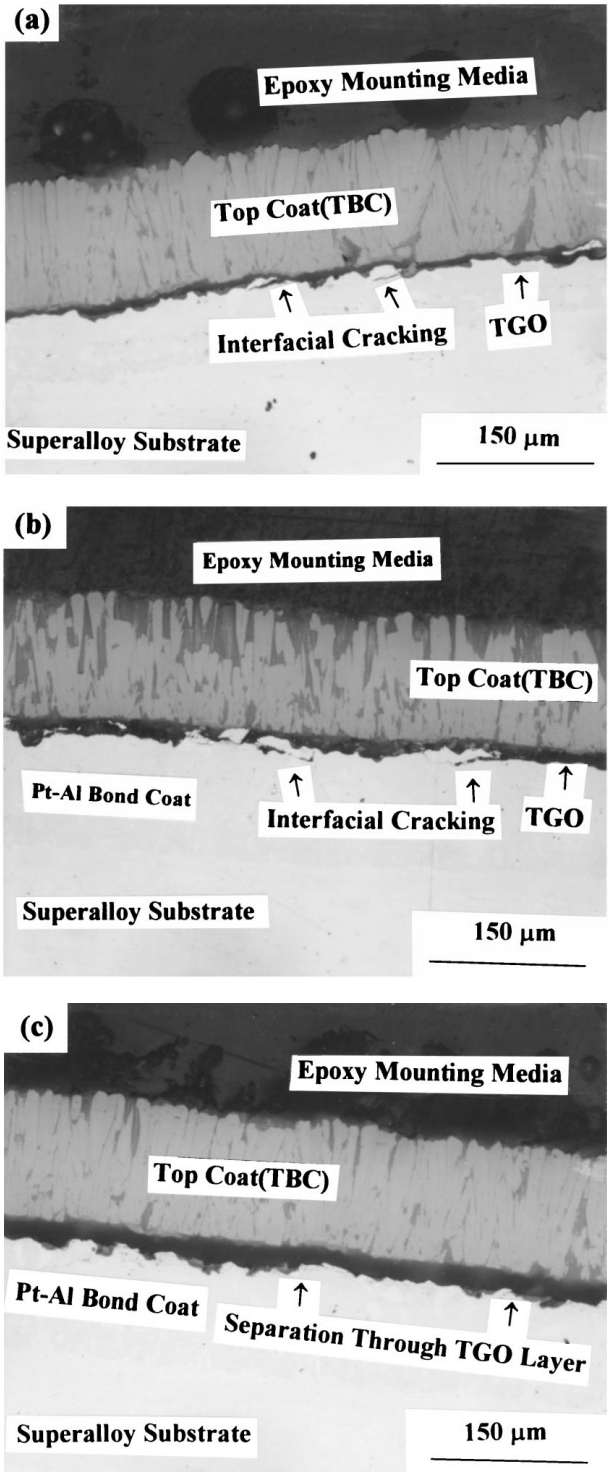

Figure 4 The optical micrographs showing the chronological evaluation of interfacial damage in TBC due to thermal cycling at 50 and 75 and 100 cycles. Separation through TGO layer is quite visible.

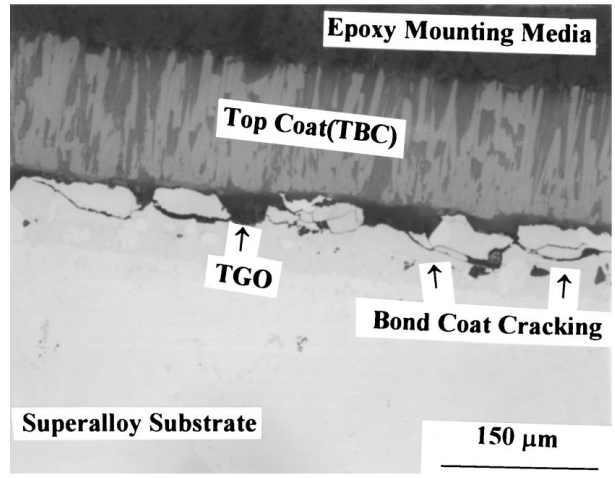

Figure 5 The photomicrograph of bond coat cracking in between bond coat and TBC after thermal cycled at 110 cycles. TGO layer is visible through the bond coat cracking. This bond coat cracking is sinusoidal nature.

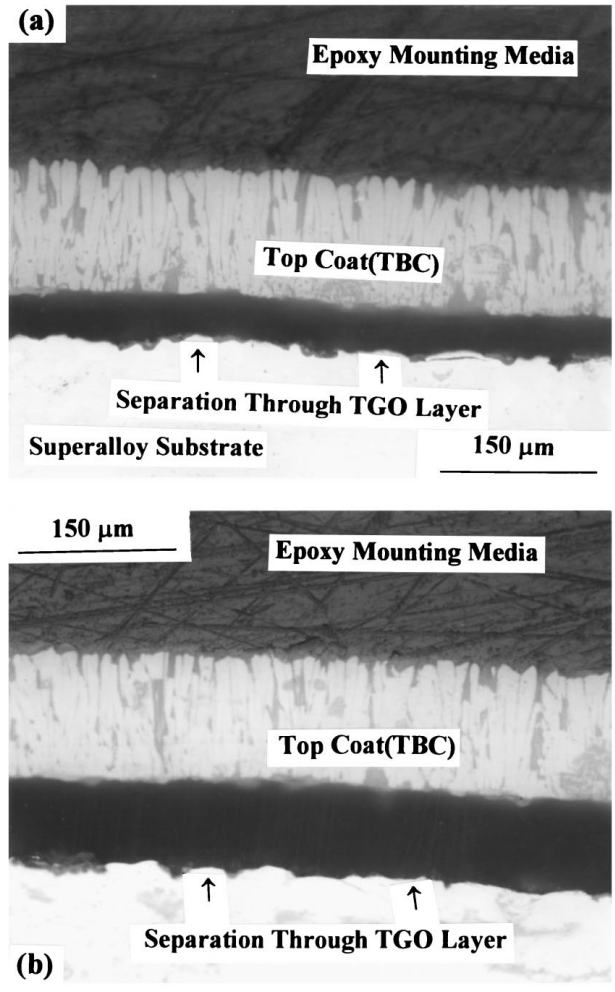

Figure 6 The optical micrographs showing complete separation through the TGO layer after thermal cycled at 175 cycles. (a) Separation at the edge of the specimen, and (b) separation at the center of the specimen.

and small at the edges of the TBC sample. The thickness of this separation at the center is roughly double that at the edges, which is ∼85.5 μm at the center and ∼42.9 μm at the edges. Fig. 7 depicts the schematic cross-section and photomicrographs of TBC specimen, showing interfacial separation through TGO layer after 150 thermal cycles. The TGO layer is thicker at the middle and thinner at the edges of the specimen. A large interfacial delamination crack is needed for buckling induced spallation to occur. Current understanding [9, 12] and from the Figs 5, 6a and b, and 7, it is now clear that buckling induced delamination is a possible mechanism for spallation.

3.2. Scanning electron microscopy (SEM)

Fig. 8a–c show the high magnification SEM micrographs taken from the specimens thermally cycled at

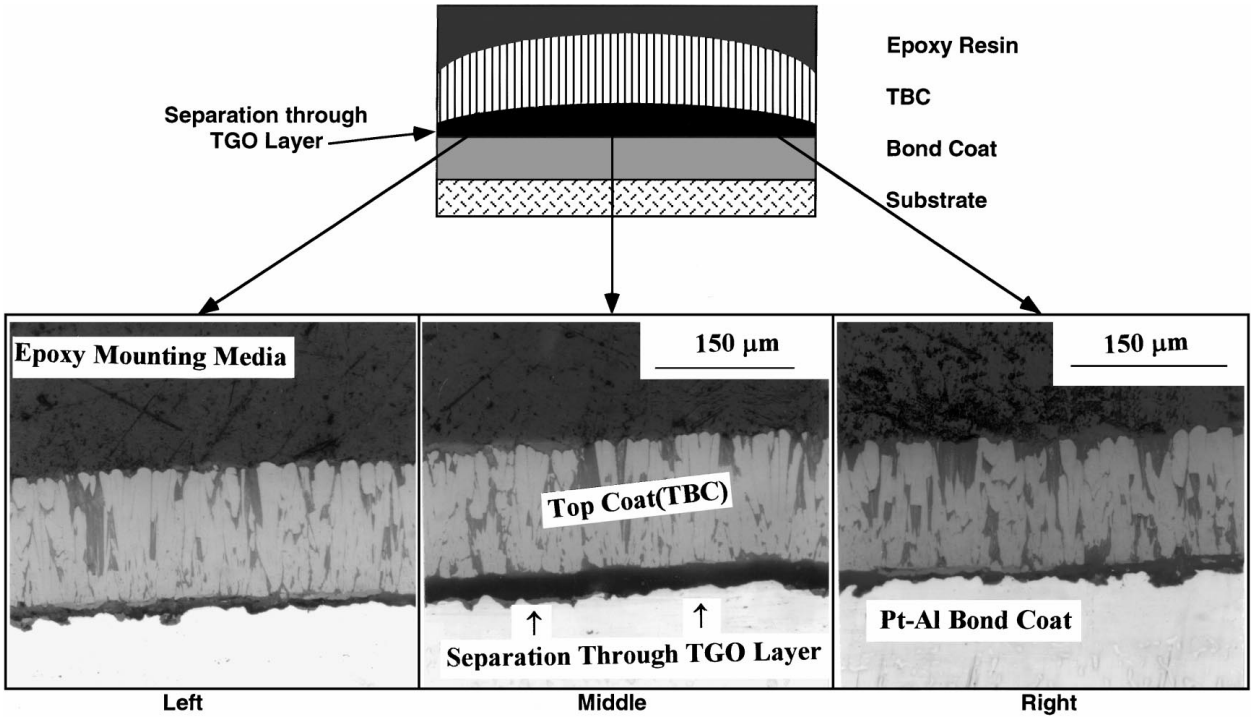

Figure 7 The schematic and photomicrographs of TBC specimen showing interfacial separation through TGO layer after thermal cycled at 150 cycles. The photomicrographs were taken from two edges and center of the specimen.

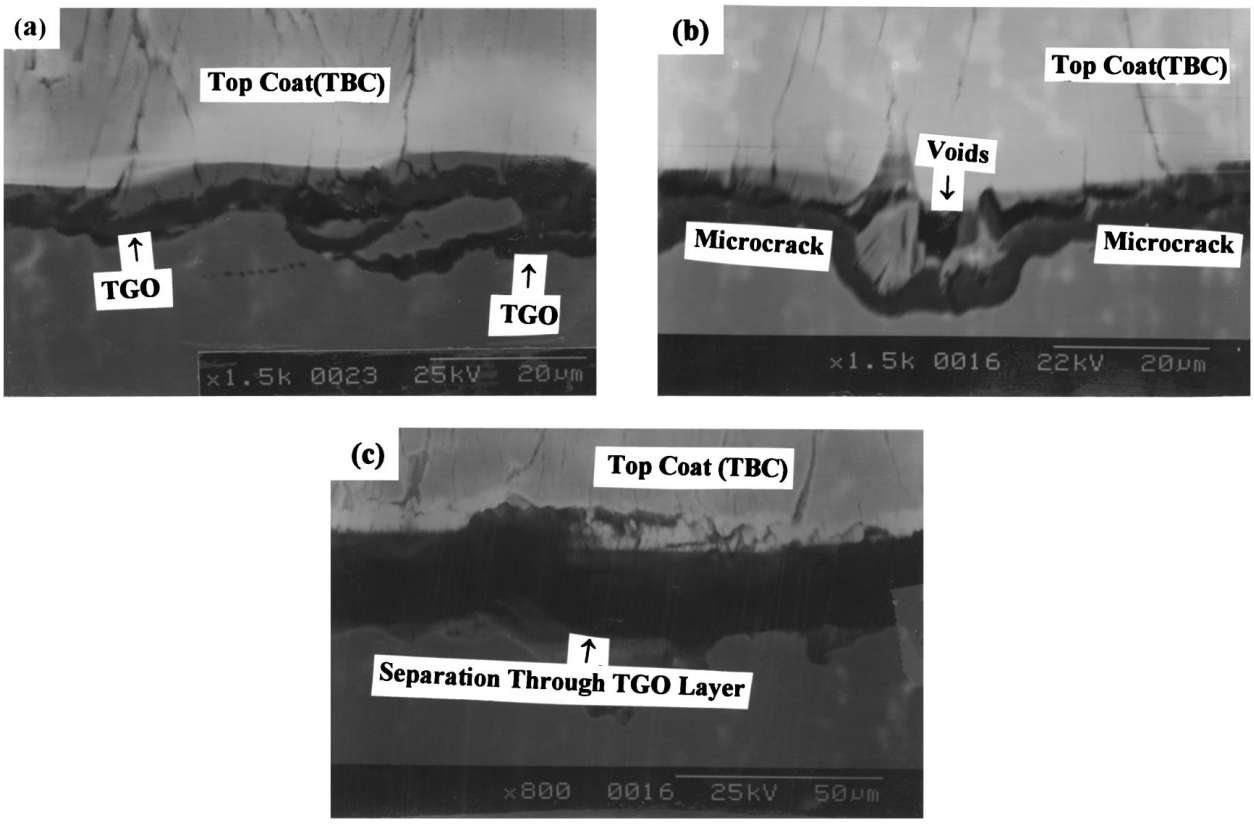

Figure 8 The scanning electron micrographs taken from the polished TBC specimens after thermal cycled at 25, 50, and 150 cycles. TGO layer, microcracks, voids, and separation through TGO layer are observed in those specimens.

25, 50, and 150 cycles. At 25 thermal cycles, separation through TGO layer is quite prominent as shown in the micrograph 8a. In micrograph 8b, voids and microcracks are seen, and TBC seems to be spalling out. Fig. 8c shows the microcrack and big separation. Interfacial damage is very large in this situation.

3.3. Nondestructive evaluation using thermal wave imaging (TWI)

Fig. 9 shows the schematic experimental set up for thermal wave imaging. This set up is used to take thermal wave image of a number of samples. Fig. 10a shows the thermal wave image of four samples at 0, 25, 50, and

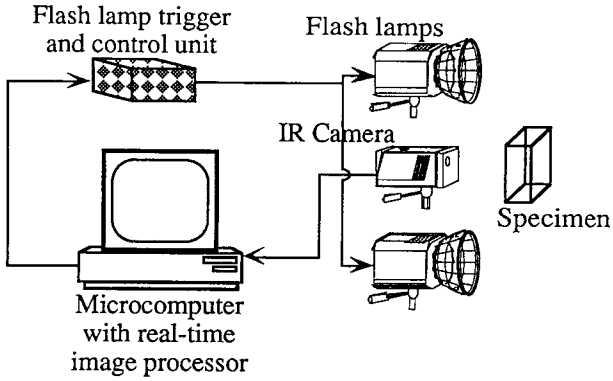

Figure 9 A schematic experimental setup for thermal wave imaging.

100 thermal cycling, respectively, from left to right. In this image map, the deeper gray levels indicate higher thermal wave signal amplitudes. The corresponding surface temperature profile plots, shown on the right-hand side of the figure, represent the relative amplitude plotted as function of position or distance across the center of the samples. The plot indicates that the thermal wave signal amplitude increases 100% from 0 thermal cycling to 25 thermal cycling, while the change in the thermal wave signal amplitude from 25 thermal cycling to 50 thermal cycling is only 10% for each case. Fig. 10b shows the thermal wave image of a second set of samples at 0, 150, and 175 thermal cycling respectively from left to right. The corresponding surface temperature profile shows that the thermal wave signal amplitude increases 150% from 0 thermal cycling to 150 thermal cycling, however, the thermal wave signal amplitudes of the 150 thermal cycling and 175 thermal cycling samples are identical. As the number of thermal cycles increases, the damage at the bond coat/top coat interface are also increased. The damage thickness may also change depending on the number of thermal cycles. This damage thickness may be responsible for the variation in the thermal wave signal amplitude.

4. Conclusions

Based on the present investigation, the following conclusions may be drawn:

1. Microcracks may occur early due to thermal cycles. A number of microcracks were observed only after two cycles (200 °C–1177 °C) in the bond coat near the TBC/bond coat interface.
2. The TGO layer continues to grow with higher the number of thermal cycles. However, there is a substantial interaction of TGO layer and damage at higher number of cycles.
3. There appears to be a transition from low-scale distribution damage (microcracks that are separate) to more extensive interlinked damage (microcracks that have connected) around 100 cycles.
4. Interfacial separation between bond coat and TBC increases with increasing the number of thermal cycles. This separation is higher at the center and lower at edges of the sample. The separation has been estimated to be 85 μm for 175 thermal cycles. This separation is twice the separation measured at the edges of the sample.
5. Based on current evidence and from our previous investigation [50], it can be concluded that buckling induced delamination is a possible mechanism for spallation.
6. Thermal wave imaging technique is a potential NDE tool to assess the degradation in TBC system.

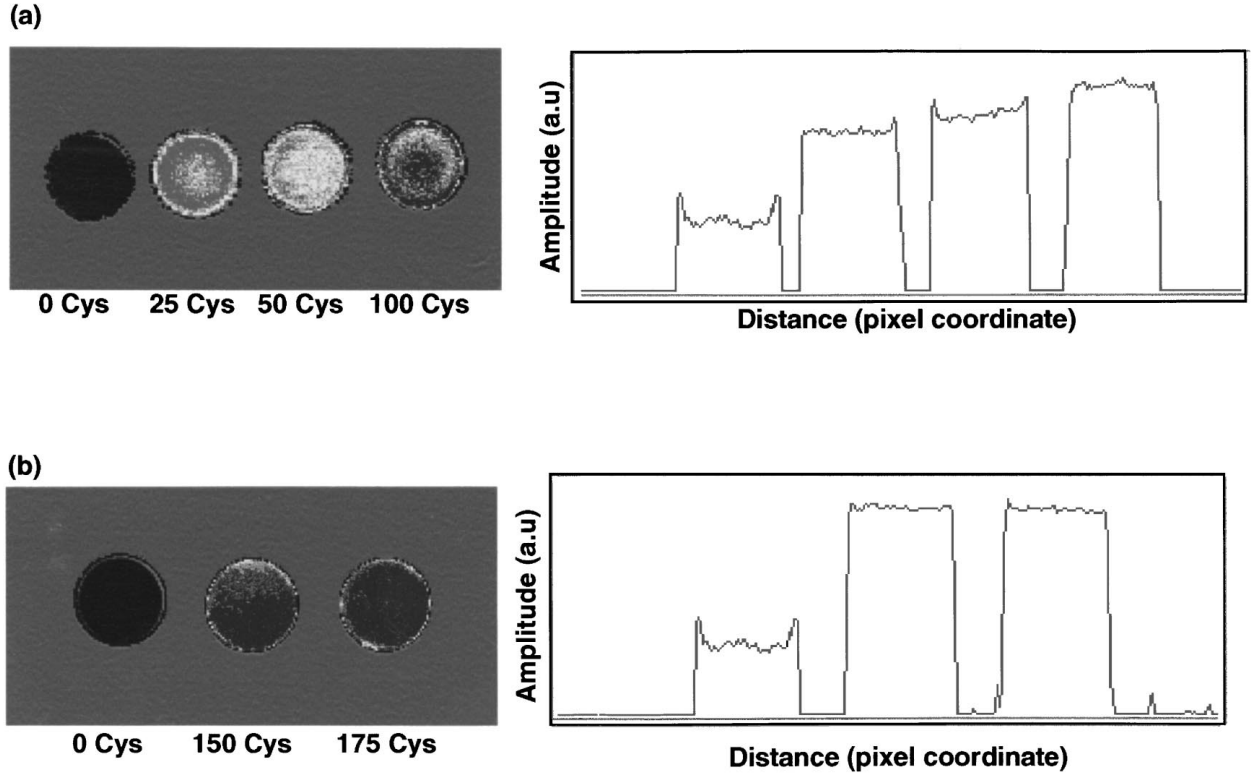

Figure 10 (a) Thermal wave image of four samples at 0, 25, 50, and 100 thermal cycles and their corresponding surface temperature profile plots, respectively, (b) thermal wave image of other set of samples at 0, 150 and 175 cycles and their corresponding surface temperature profile plots.

Acknowledgements

This program was funded by Air Force Office of Scientific Research-grant # F 49620-95-1-0201 (Dr. Walter Jones, Program Monitor). Dr. Kennard P. Wright of GE Aircraft Engines is acknowledged for his support with samples and fruitful comments during the course of this investigation.

References

1. R. A. MILLER and C. E. LOWELL, *Thin Solid Films* **99** (1982) 265.
2. K. D. SHEFFLER and D. K. GUPTA, "The American Society of Mechanical Engineers," 88-GT-286.
3. E. DEMARAY, DOE Contract DE-AC-06-76RL01830, 1982 (Department of Energy).
4. D. S. DUVALL, 1982, in Proceedings from the Second Conference on Advanced Materials for Fuel Capable Heat Engines (Electric Power Research Institute, Palo Alto, CA EPRI-RD-2396-SR) p. 6.
5. M. F. STROOSNIJDER, M. J. BENNET and R. MEVREL, "Advanced Technologies for Surface Engineering," (1992) 335.
6. C. MERTENS, D. MUCK and J. GARCIA, "Materials for Advanced Power Engineering, Part II," 1994, 1313.
7. M. GOBEL, A. RAMEL, M. SCHUTZE, M. SCHORR and W. T. WU, *Mater. at High Temp.* **12** (1994) 301.
8. E. J. FELTEN and F. S. PETTIT, *Oxidation of Metals* **10**, (1976) 189.
9. H. E. EVANS, *Mater. Sci. Eng.* **A120** (1989) 139.
10. R. A. MILLER and C. E. LOWELL, *Thin Solid Films* **95** (1982), 265.
11. W. R. SEVICK and B. L. STONER, NASA Contractor Report, CR-135360, 1978.
12. A. G. EVANS, G. B. GRUMLEY and R. F. DEMARY, *Oxidation of Metals* **20** (1983), 193.
13. J. R. SPRINGARAN, B. E. JACOBSON and W. D. NIX, *Thin Solid Films* **45** (1977) 507.
14. R. A. MILLER and C. E. LOWEL, NASA TM-82905 (1982).
15. S. STECURA, NASA TM-79206, (1979).
16. M. A. GEDWILL, NASA TM-81567, (1980).
17. R. A. MILLER and C. BERNDT, NASA TM-83663, (1984).
18. C. H. LIEBERT and R. MILLER, I & EC Product Research and Development, Sept. (1984) 334.
19. S. R. LEVINE, R. MILLER and P. E. HODGE, *Sampe Quarterly* **12** (1980) 20.
20. S. R. LEVINE and R. MILLER, *Research and Development* **26** (1984) 122.
21. Y. R. TAKEUCHI and K. KOKINI, Trans. of the ASME **116** (1994) 266.
22. Proceedings of the Coatings for Advanced Heat Engines workshop, (US DOE, Castine, Maine, 1987).
23. Proceedings of the 1992 Coatings for advanced Heat Engines Workshop (US DOE Monterey, California, 1992).
24. J. T. DEMASI, K. D. SHEFFLER and M. ORTIZ, NASA Contractor Report 182230, prepared for NASA under contract NAS3-239544, December (1989).
25. S. M. MEIER, D. M. NISSLEY and K. D. SHEFFLER, NASA Contractor Report 189111, prepared for NASA under Contract NAS3-23944, July (1991).
26. R. A. MILLER, W. J. BRINDLEY, J. G. GOEDJEN, R. TIWARI and D. MESS, Proceedings of the 7th National Thermal Spray Conference (Boston, Massachusetts, June 20–24, 1994).
28. R. A. MILLER and W. J. BRINDLEY, in Proceedings of the International Thermal Spray Conference & Exposition (Orlando, Florida, May 28–June 5, 1992).
29. G. MCDONALD and R. C. HENDRICKS, NASA TM-81480 (1980).
30. J. W. WATSON and S. R. LEVINE, NASA TM 83670, (1980).
31. 1983 Independent Research and Development Plan, General Electric Company, Aircraft Engine Business Group, R83 AEB263, Vol. V, (1983).
32. S. RANGASWAMY, H. HERMAN and S. SAFI, *Thin Solid Films* **73** (1980) 43.
33. P. F. BECHER, R. W. RICE, C. C. WU and R. L. JONES *ibid.* **53** (1978) 225.
34. R. C. BILL, NASA TM-81732 (1981).
35. R. L. MULLEN, G. MCDONALD, R. C. HENDRICKS and M. HOFLE, NASA TM-83460 (1983).
36. J. R. SPRINGARAN, B. E. JACOBSON and W. D. NIX, *Thin Solid Films* **45** (1977) 507.
37. C. A. ANDERSON, R. J. BRATTON, S. K. LAU and S. Y. LEE, in International Conference on Metallurgical Coatings, Elsevier Sequoias, Laussane (San Diego, California, April, 1980).
38. R. A. MILLER, S. R. LEVINE and P. E. HODGE, in Proceedings 4th International Symposium on Superalloys, Seven Springs, PA, September, 1980 (ASM, Metals Park, OH 1980) p. 473.
39. R. A. MILLER, S. R. LEVINE and S. STECURA, Paper # AIAA 80-0302, AIAA Meeting (Pasadena, CA, Jan. 1980).
40. S. STECURA, in International Conference on Metallurgical Coatings (Elsevier Sequoia, San Diego, April 1980), 481.
41. N. R. SANKAR, C. C. BRENDT and H. HERMAN, *Ceramic Eng. Sci. and Proc.* **4** (1983) 784.
42. C. H. LIEBERT, *Thin Solid Films* **64** (1979) 329.
43. R. C. HENDRICKS, G. MCDONALD and R. L. MULLEN, *ibid.* **4** (1983) 802.
44. Proceedings of the 1987 Coatings for Advanced Heat Engines Workshop, US DOE, Castine, Maine (1987).
45. Proceedings of the 1992 Coatings for Advanced Heat Engines Workshop, US DOE, Monterey, California.
46. R. V. LANG, F. JAMARNI, K. L. YAN and M. N. KOROTKIN, in 3rd International SAMPE Metals Conference, October 1992.
47. Z. A. CHAUDHURY, G. M. NEWAZ and T. AHMED, *J. of Mat. Letters* **17** (1998) 85.
48. Z. A. CHAUDHURY, G. M. NEWAZ, S. Q. NUSIER and T. AHMED, *J. of Mat. Sci. Eng.* **A231** (1997) 34.
49. Z. A. CHAUDHURY and G. M. NEWAZ (unpublished work).
50. G. M. NEWAZ, S. Q. NUSIER and Z. A. CHAUDHURY *J. Eng. Mat. and Tech.* **120** (1998) 149.
51. L. LELAIT, S. ALPERINE and R. MEVREL, *J. Mater. Sci.* **27** (1992) 5.
52. E. Y. LEE, R. R. BIEDERMAN and R. D. SISSON, *J. Mat. Sci. Eng.* **A 121** (1989) 467.
53. P. A. SIEMERS and W. B. HILLIG, NASA CR-165351, (1981).

Received 4 November 1996
and accepted 12 February 1998